Spatially-Continuous Plantar Pressure Reconstruction Using Compressive Sensing

Amirreza Farnoosh and Sarah Ostadabbas FARNOOSH.A@HUSKY.NEU.EDU, OSTADABBAS@ECE.NEU.EDU
Electrical & Computer Engineering Department, Northeastern University
360 Huntington Avenue, Boston, MA 02115, USA

Mehrdad Nourani NOURANI@UTDALLAS.EDU
Electrical & Computer Engineering Department, The University of Texas at Dallas
800 West Campbell Road, Richardson, TX 75080, USA

Abstract

Wearable technologies can benefit from compressive sensing (CS) as an efficient signal transformation, compression, and reconstruction technique. Among such technologies, in-shoe pressure monitoring systems are designed to continuously record plantar pressure distribution for various applications ranging from medical research to product development in sports and healthcare. To gather adequate information from plantar area, a high resolution spatial pressure reading is required. However, to achieve a practical wearable monitoring system with long battery life at a reasonable price, the number of sensors in the shoe must be very limited. In this paper, we employed CS principles to reconstruct spatially-continuous plantar pressure distribution from a small number of sensors (i.e. $K < 10$) based on a supervised dictionary learning approach. The learned dictionary transforms the high-resolution pressure distribution to a sparse representation which is accurately reconstructable using either orthogonal matching pursuit (OMP) or least absolute shrinkage and selection operator (LASSO) algorithm. Using plantar pressure data from 5 participants, we demonstrated that our method outperforms grid-based and non-gridded interpolation techniques even at $K = 4$ sensors such that the best interpolation needs more than $K = 170$ sensors to give the same reconstruction accuracy. With $K = 4$ sensors, we achieved a root mean squares (RMS) reconstruction error of 6.7 kPa per sensing cell while the error remained below 16 kPa for pressure values up to 160 kPa. Our algorithm is also shown to be robust in presence of measurement error and limited training data, therefore efficiently addresses the challenges encountered in production of commercial in-shoe monitoring systems.

1. Introduction

Compressive Sensing (CS) is an l_1-norm minimization-based signal transformation, compression, and reconstruction approach that provides a sparse representation of the information presented in the original signal. CS yields a more efficient representation of the original signal with a relatively smaller number of projected components for information reconstruction compared to classical techniques. This feature allows for a lower sampling rate than the Nyquist without losing information in the original signals (Candès and Wakin, 2008). Previous studies have shown the practical value of CS as a power efficient signal reconstruction technique particularly for body sensor networks and wearable monitoring technologies

(Craven et al., 2015; Liu et al., 2014; Williamson et al., 2015; Xu et al., 2012; Zhang and Sawchuk, 2013). One wearable technology that could benefit from CS compression and reconstruction efficiency is in-shoe plantar pressure monitoring which has various applications ranging from medical research to product development in sports and healthcare.

1.1 Plantar Pressure Monitoring Applications

Plantar pressure monitoring systems have been used by researchers in gait analysis to enhance footwear or therapeutic orthotics designs (Abdul Razak et al., 2012). It provides valuable insight for professional athletes who seek to maximize their performance or prevent injuries with appropriate feedback about incorrect foot position or warns of exhaustion and overload. It is also used to coach patients in walking rehabilitation exercises through provision of distribution measurement in the form of visual feedback (Wada et al., 2010). Plantar pressure distribution provides key insights into foot function to help identify pathologies, as well as aiding in prevention and treatment of wounds caused by high foot pressure specially for diabetic patients. A vast majority of diabetic patients suffer from foot problems like degenerative foot disorder and complications due to neuropathy. An inability to feel pain due to prolonged high pressure being placed upon the feet creates the conditions for serious foot problems, mainly ulcers. Diabetic foot ulcers are responsible for more hospitalizations than any other complication of diabetes (Rice et al., 2014). Therefore, an assistive technology able to automatically measure the force applied to the foot throughout the day would be a significant asset to the foot ulcer prevention field. By embedding advanced miniaturized force sensors in shoe insoles, plantar pressure distribution can be collected wirelessly in realtime. These recorded pressure data could be used for diabetic and neuropathic patients' feet screening, orthotics and prosthetics efficacy profiling, pre- and post-surgical comparative analysis, and degenerative foot disorder monitoring.

1.2 Current Technologies

Several plantar pressure mapping systems are commercially available, among which are the Go-tec (SPI) and F-Scan (TEK). Such systems cost thousands of dollars per unit and are mostly aimed for in-lab applications. There are also a number of sensor-insole products in which a limited number of sensors are integrated into footwear at few regions of plantar area. PPS pressure sensing booties employ 25 sensing elements and were originally designed for research in surf science (PPS). OpenGo insole from Moticon consists of 13 relatively large pressure sensors with 50% coverage throughout the footprint and targets skiers as users for realtime audio coaching during their run (MOT). InsoleX from Sennotech, although having only 48 wireless sensors embedded in footwear costs around several thousands (SEN). In addition to their expensive price, such technologies suffer from poor spatial resolution and underestimation of peak pressures. In fact, except for a few exact points under the sensors, pressure distribution information on other parts of the plantar area is completely lost.

A practical in-shoe pressure monitoring technology needs to satisfy both wearability and accuracy requirements. The number of sensors embedded in shoe is a deciding factor in design which directly influences power consumption (i.e. battery size and weight), plantar area coverage (i.e. measurement accuracy), and also the final product price. Therefore, an affordable in-shoe monitoring system is expected to consist of limited numbers of sensors

(e.g. 10 or less), carefully placed in the locations that a high resolution pressure image can be estimated from their readings. There have been only a few attempts to address the reconstruction of plantar pressure from sparse number of sensors. In a previous work, authors investigated possibility of finding an optimum sparse sensor placement to minimize reconstruction error (Ostadabbas et al., 2012a,b). In a followup study, they proposed a knowledge-based Gaussian mixture model approach accompanied with a PCA-based model order reduction for image reconstruction from sparse number of sensors and obtained reasonable reconstruction accuracy by using only 10 sensors (Ostadabbas et al., 2014).

2. Spatially-Continuous Plantar Pressure Reconstruction

In order to achieve a practically useful wearable plantar pressure monitoring system with high spatial resolution, long battery life between charges, and at a reasonable price point, the number of sensors in the shoe should be very limited. We employed a compressive sensing technique to reconstruct a spatially-continuous plantar pressure distribution using data collected from a limited set of pressure sensors embedded in the shoe.

2.1 Problem Formulation

A spatially-continuous plantar pressure distribution, $\mathcal{Q}_i$ at a given time instance, t_i, needs to be reconstructed from a sparse set of K location-known pressure sensor readings, p_j for $j \in \{1, \ldots, K\}$. Let's assume each $\mathcal{Q}$ has been evenly discretized to an $n_1 \times n_2$ grid-based pressure image, in which column-stacking of pixels results in an $N = n_1 \times n_2$ vector, $\mathcal{X}$. The problem of reconstructing vector $\mathcal{X}$ from K sensor readings, $\mathcal{P} = [p_1, p_2, \ldots, p_K]^T$, when $K << N$ is reduced to solving the following under-determined linear equations:

$$\mathcal{P} = \mathcal{A}\mathcal{X} \tag{1}$$

where $\mathcal{A}$ is a binary $K \times N$ *selection* matrix with non-zero elements only on predefined sensor locations. It is worth noting that the under-determined system of Equation (1) has many possible solutions since the number of observations (sensor values) is less than the number of unknowns. However, we may search for a sparse solution by assuming sparsity of $\mathcal{X}$ in the original or a transformed domain. We denote $\hat{\mathcal{X}}$ to be the sparse representation of $\mathcal{X}$ such that $\mathcal{X} = \Psi\hat{\mathcal{X}}$, and re-write Equation (1) as:

$$\mathcal{P} = \mathcal{A}\Psi\hat{\mathcal{X}} \tag{2}$$

where Ψ is an $N \times N'$ *basis* or *dictionary* matrix ($K << N'$) and $\hat{\mathcal{X}}$ is a vector of length N' which has at most S number of non-zero elements. $A\Psi$ is called *mixing* matrix. At this point, Equation (2) can be solved for $\hat{\mathcal{X}}$ and once we have $\hat{\mathcal{X}}$, we can find $\mathcal{X} = \Psi\hat{\mathcal{X}}$. Based on the type of dictionary, N' can be equal, smaller or greater than N. In our experiment, we chose transformations which result in $N' \leq N$.

2.2 Finding A Sparse Solution

The sparsest solution to the under-determined Equation (2) is achieved through solving the following constrained optimization problem:

$$\underset{\hat{\mathcal{X}}}{\text{minimize}} \quad \|\hat{\mathcal{X}}\|_0, \quad \text{subject to} \quad \mathcal{P} = \mathcal{A}\Psi\hat{\mathcal{X}} \tag{3}$$

where norm $\|.\|_0$ counts the number of non-zero entries. Equation (3) is not a convex optimization problem and may not have a unique solution. Theoretically, if there is a feasible solution that satisfies $\|\hat{\mathcal{X}}\|_0 < (1 + \mu^{-1}(A\Psi))/2$, then $\hat{\mathcal{X}}$ is the unique sparsest solution to Equation (3) and its l_1 relaxation (Donoho and Elad, 2003). Here, $\mu(.)$ is the *mutual coherence* of a matrix, which is the largest absolute normalized inner product (correlation coefficient) among all pairs of matrix columns.

It is often challenging to find a concise underlying sparse representation for sensor data especially when a complex dynamics such as human motion is the source of the data. Assuming that the transformed data $\hat{\mathcal{X}}$ has most (but not necessarily all) of its energy concentrated in a relatively small number of coordinates in the new basis Ψ, we can generalize sparsity to a wider class of signals and still recover data with a high accuracy. By enforcing the desired level of sparsity, S, and allowing the equality in Equation (2) to deviate with respect to some error, the optimization problem in Equation (3) turns into:

$$\underset{\hat{\mathcal{X}}}{\text{minimize}} \quad \|\mathcal{P} - \mathcal{A}\Psi\hat{\mathcal{X}}\|_2^2, \quad \text{subject to} \quad \|\hat{\mathcal{X}}\|_0 \leq S \tag{4}$$

This formulation is also valid for $K \geq N'$ when some level of error is accepted for the sake of a sparse solution. This optimization problem has non-deterministic polynomial-time complexity (NP-hard) and thus it is computationally intensive to find an valid sparse solution even for relatively short length vectors.

Several methods have been proposed in the CS literature for solving the problem of l_0-norm sparse recovery using approximation techniques to the algorithms with polynomial complexity (Candès and Wakin, 2008). For our application, we implemented the stage-wise orthogonal matching pursuit (OMP) algorithm (Donoho et al., 2012), which is among the most efficient classical approaches for finding sparse solutions. This non-convex problem can also be formulated as a regularized l_1-norm optimization problem and solved using the well-established least absolute shrinkage and selection operator (LASSO) algorithm (Tibshirani, 1996). Researchers have proven that when sparsity level is not too big, solutions of l_1-norm minimizer coincide with that of the l_0-norm minimizer (Donoho and Elad, 2003).

2.3 Dictionary Learning and Reconstruction

The main question arising at this point is the optimal choice of a basis matrix or dictionary Ψ, in which our data can be approximated with a sparse representation. One idea is choosing a pre-designed dictionary such as discrete cosine transform (DCT) or discrete wavelet transform (DWT), which have shown promising results in colored image compression. However, such transformations are not fine-tuned for specific types of data and are not satisfactory especially when an extremely sparse representation is desired. Elad et al. proposed an effective singular value decomposition (SVD)-based method of training dictionaries for data-specific sparse representation (Aharon et al., 2006). The K-SVD algorithm is an iterative learning method that refines an initial dictionary to better fit the data with respect to a desired sparsity level. K-SVD uses sparse coding of the high resolution training samples to solve the following optimization problem:

$$\underset{\hat{\mathbf{X}},\Psi}{\text{minimize}} \quad \|\mathbf{X} - \Psi\hat{\mathbf{X}}\|_2^2, \quad \text{subject to} \quad \|\hat{\mathcal{X}}_i\|_0 \leq S \quad \forall i = 1, \ldots, M \tag{5}$$

where $\mathbf{X} = [\mathcal{X}_1, \ldots, \mathcal{X}_M]$ contains M high resolution training data and $\hat{\mathbf{X}} = [\hat{\mathcal{X}}_1, \ldots, \hat{\mathcal{X}}_M]$ represents their corresponding sparse representation with respect to $\Psi = [\psi_1, \ldots, \psi_{N'}]$. The algorithm starts with an existing dictionary Ψ_0 (that can be formed by random selection from training data) and then finds/updates $\hat{\mathbf{X}}$ and Ψ consecutively in a two-step process at each iteration as shown in Algorithm. 1.

Data: $\mathbf{X}$ (training data), Ψ_0 (initial dictionary), N' (# of dictionary columns), S (desired sparsity level), I (# of iterations)
Result: Ψ (dictionary)
initialization: $\Psi = \Psi_0$, $i = 0$;
while $i < I$ **do**
1 **Sparse Coding:** Fix Ψ and find S-sparse solutions, $\hat{\mathbf{X}}$, to Equation (5) using OMP algorithm;
2 **Dictionary Update:** $j = 1$;
while $j \leq N'$ **do**
3 Find column indexes in $\hat{\mathbf{X}}$ that have non-zero coefficients for dictionary column, ψ_j, and denote them by $\{t\}$;
4 Set ψ_j (column j in Ψ) to zero;
5 $U\Sigma V^T = \mathbf{SVD}(\mathbf{X}_{\{t\}} - \Psi\hat{\mathbf{X}}_{\{t\}})$; let σ_1 be the largest singular value and u_1, v_1 its corresponding singular vectors;
6 Update $\psi_j = u_1$ and its corresponding coefficients in $\hat{\mathbf{X}}$ with $\sigma_1 v_1$;
7 $j = j + 1$;
end
8 $i = i + 1$
end

Algorithm 1: K-SVD Algorithm

We propose a slight modification in the classical K-SVD algorithm to include the effect of the selection matrix, $\mathcal{A}$, in the learning phase. Our modified K-SVD algorithm finds S-sparse OMP solutions, $\hat{\mathbf{X}}$, that minimize $\|\mathcal{A}\mathbf{X} - \mathcal{A}\Psi\hat{\mathbf{X}}\|_2$ for a fixed dictionary in the 'Sparse Coding' step, but still keeps the 'Dictionary Update' step as before. This modification is intelligible since this setting follows the sparse reconstruction formulation of Equation (4) and generally there is no guarantee that OMP solutions with all sensor values (as in classical K-SVD) coincide with those obtained using sparse number of sensors. After learning the dictionary, Ψ, on a training set, Equation (4) is solved for a test image to obtain $\hat{\mathcal{X}}$, and once we have $\hat{\mathcal{X}}$, $\mathcal{X} = \Psi\hat{\mathcal{X}}$ is calculated. A block diagram of dictionary learning and image reconstruction procedure is shown in Figure 1.

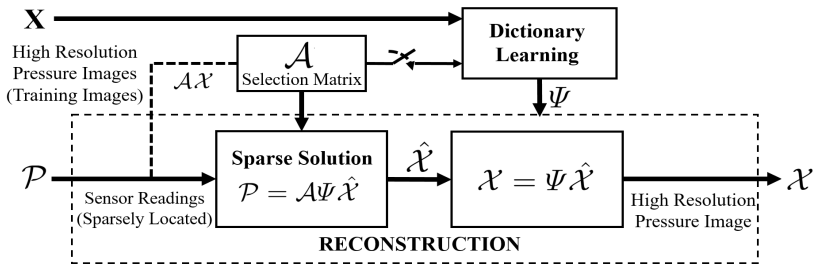

Figure 1: Block diagram of dictionary learning and image reconstruction.

3. Experimental Investigation

3.1 Experimental Setting

In order to investigate the performance of the proposed algorithm, we utilized experimental plantar pressure data collected at the University of Texas at Dallas from 5 healthy participants (2 females and 3 males) with details provided in (Ostadabbas et al., 2014). The high resolution pressure data was obtained using a pressure measurement platform with the area of 435.9×368.8 mm^2 manufactured by Tekscan (TEK). This floor mat consists of evenly spaced resistive force sensors of sensing area equals to 8.4×8.4 mm^2, which can measure up to 862kPa. Participants (19-51 years old) were asked to walk normally across the pressure mat for two minutes and pressure data was sampled at 50Hz.

3.2 Preprocessing

We used the same preprocessing procedure provided in (Ostadabbas et al., 2014) to prepare the pressure data for our analysis pipeline. Please note that the preprocessing phase is not required if the high resolution data is collected from an in-shoe pressure insole.

Stage 1: Step Splitting – In the first stage, we separate individual steps and label them as right or left step for each participant. Each individual step includes a series of frames in tandem during a gait cycle. An individual *step image* is obtained by selecting the maximum pressure value for each pixel among all frames in a given step.

Stage 2: Image Registration – In this stage, we align pressure images of individual steps for each person. All step images of a participant's left or right foot are registered to the first image in the set of step images through rotational and translational alignment.

Finally, for each participant, we randomly marked 70% of the steps as training data for data-driven model extraction and the rest as test data to evaluate the performance of our proposed reconstruction algorithms. After preprocessing, the image frames of size 20×37 pressure-pixels were built with details provided in Table 1 for each participant.

3.3 Sensor Location Selection

Human plantar area can be divided into four key regions which are known to experience high pressures during a complete gait cycle: big toe, heel, first metatarsal head and fourth/fifth metatarsal heads. They are also medically important due to their vulnerability in developing foot ulcers especially in neuropathic patients (Lavery et al., 2008). It is reasonable to have at

Table 1: Collected pressure data from each participant

Participant	Foot	No. of Gait Cycles	No. of Training Frames	No. of Test Frames
#1	Left	71	2485	867
	Right	70	2513	836
#2	Left	70	2512	797
	Right	70	2505	853
#3	Left	44	2431	808
	Right	44	2397	797
#4	Left	56	2436	809
	Right	55	2431	836
#5	Left	34	2463	787
	Right	34	2246	839

least one sensor reading from each of these regions. These regions were manually determined by a medical technician for each participant based on visual inspection of the pressure data and were included in the dataset. In our experiments, for each participant's foot, in each of the four plantar regions, we selected a sensor location that experienced peak values among all training step images and then chose the remaining sensor locations randomly.

3.4 Reconstruction Error Measurement

In this study, we used root mean squares (RMS) error as the measure of the deviation of the reconstructed pressure image from its ground truth. For each participant's foot, we calculated RMS error along all nonzero pixels within the step images of all gait cycles in the test set. We evaluated RMS error at each K (number of sensors) for 10 random sets of sensors selected as described in Section 3.3. To report the overall RMS error among all participants' foot pressure data in Section 3.5, we chose the sensor sets with median RMS error at each K and then evaluated error along reconstructed images from all participants.

3.5 Experimental Results

The main objective of this study is to achieve accurate reconstruction of high resolution plantar pressure images from $K < 10$ number of pressure sensor readings. To make this possible, the sparsity level S in the transformed domain, $\hat{\mathcal{X}}$, should be less than the number of sensors, i.e., $S < K$. Our experimental analysis is performed by: (1) picking only $K \geq 4$ sensor locations from a high resolution test pressure image, (2) selecting or learning dictionary Ψ, (3) reconstruction using proposed algorithms, and finally (4) calculating reconstruction error with respect to the high resolution ground-truth test pressure image.

3.5.1 Reconstruction using DCT dictionary

Figure 2 shows reconstruction error versus number of sensors using a complete 2-dimensional DCT dictionary of size 740×740. OMP algorithm with $S = 4$ and LASSO were used in the reconstruction phase. Due to LASSO algorithm increasing computational cost, only the results for up to 24 sensors are shown. Although LASSO surpassed OMP in reconstruction accuracy, neither of the algorithms was truly successful since the pressure images are not indeed sparse enough in the DCT domain. To make it clear, on average, more than 35% of the image energy is lost when only 24 largest coefficients in the DCT domain are considered and thus it highlights the importance of learning a proper dictionary.

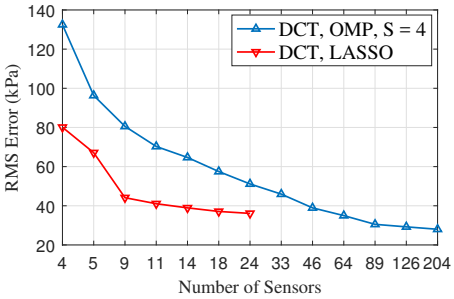

Figure 2: Reconstruction error using 740×740 DCT dictionary.

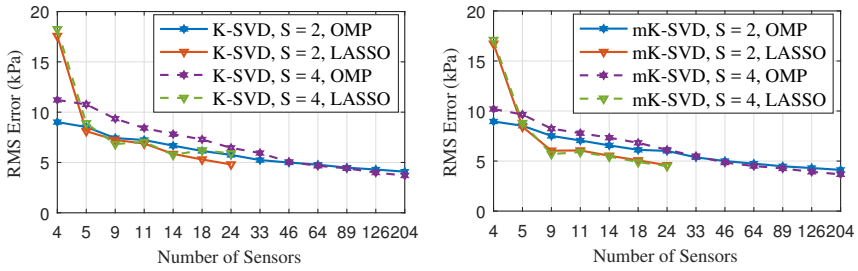

(a) Classical K-SVD **(b)** mK-SVD

Figure 3: Reconstruction error using 740×740 learned dictionaries.

3.5.2 Reconstruction using K-SVD learned dictionary

The results of using 740×740 dictionaries learned by classical and modified K-SVD (mK-SVD) algorithms with $S = 2, 4$ are shown in Figure 3. In the mK-SVD (which sensor locations are considered in the learning phase), we used learned dictionaries with $K = 4$ for all cases. In the reconstruction phase, we enforced the same sparsity level used in the learning phase for OMP. The best results were obtained for dictionaries learned with $S = 2$ and when OMP was used for reconstruction. The results for $S = 2$ are better than $S = 4$ for smaller number of sensors ($K < 46$). This is consistent with the theoretical finding that the algorithms perform better when S is smaller, in which sparse reconstruction constraints are more likely to be satisfied (Donoho and Elad, 2003).

The reconstruction error for LASSO reduces significantly from $K = 4$ to $K = 5$ sensors. To further explore the reason, we computed pairwise correlations between columns of each dictionary Ψ and noticed that, on average, about 20% of the columns have correlation more than 0.9. This percentage drops significantly from 38% in mixing matrix, $\mathcal{A}\Psi$, with $K = 4$ to 25% with $K = 5$, which is apparently much closer to its value in complete dictionary. Note that the more correlated the columns of $\mathcal{A}\Psi$, the less chance we have to reconstruct images using LASSO (see mutual coherence in Section 2.2). As shown in Figure 3, OMP and LASSO perform better using the dictionaries learned by mK-SVD, but the margin is insignificant for OMP with $S = 2$. This is mainly because its dictionary columns are highly correlated (rank of dictionaries is less than 400). This fact results in reducing the dictionary columns which in turn drastically decreases computational cost in the reconstruction phase. We learned dictionaries with only 50 columns (size of 740×50) using classical and modified K-SVD with $S = 2$. We also confined the analysis to OMP due to its simple implementation and low computational cost, which is critical for realtime applications. The results are shown in Figure 4(a). This dimensionality reduction has trivial effect on reconstruction error when using dictionaries learned by classical K-SVD (gives almost the same results as for complete dictionaries especially for $K \leq 14$ sensors). However, the mK-SVD algorithm clearly outperformed the classical version at this dimension.

3.5.3 Reconstruction using different sensor sizes

For this part of experiment, we employed high resolution pressure data with small gridded sensors for the learning phase, but instead utilized larger insole sensors for reconstruction, since larger force sensors are usually manufactured with lower cost. We implemented this configuration in reconstruction by collecting the average pressure value around a sensor

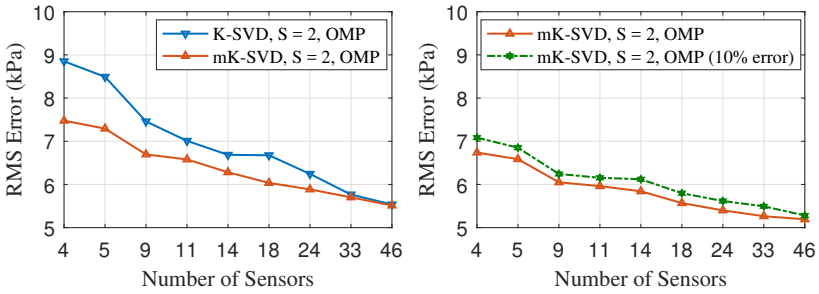

(a) Small sensors **(b)** Large sensors

Figure 4: Reconstruction error using 740×50 dictionaries learned by classical K-SVD and mK-SVD.

location, instead of reading pressure value at the sensor itself, through modifying the selection matrix $\mathcal{A}$. In this way, we included information from adjacent locations and have a better conditioned mixing matrix $\mathcal{A}\Psi$ while preserving the same number of sensors. We used mK-SVD with $S = 2$ and applied non-overlapping 3×3 averaging windows (9 times larger sensors) centered on each selected location. The result in Figure 4(b) shows clear improvement in reconstruction accuracy (solid line). To address the sensitivity issue of the system due to the use of different sensor types in learning and reconstruction, we added random errors up to $\pm 5\%$ to the average values and then reconstructed images. The result in Figure 4(b) (dotted line) shows that we still have a better reconstruction accuracy.

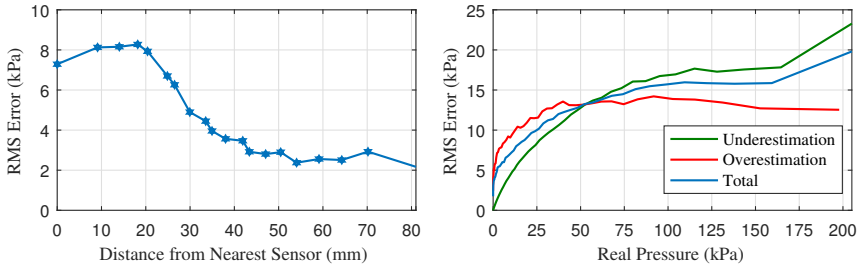

(a) **(b)**

Figure 5: Error as a function of (a) distance to nearest sensor, and (b) real pressure for $K = 4$, 740×50 dictionaries, mK-SVD with $S = 2$ and OMP.

3.5.4 Error as a function of distance & real pressure

Figure 5(a) shows error as a function of distance from the nearest sensor for $K = 4$. The error has a low rise at close distances because the model attempts to fit on the known values and then starts dropping at $20mm$ because the farther away from sensor locations, regions are more likely to experience lower pressures. We obtained this graph by sorting and dividing distances into 20 bins with nearly equal data points and then reported the RMS error and average distance for each bin. Figure 5(b) shows RMS error as a function of real pressure value for $K = 4$ and determines the contribution of overestimation and underestimation to the error. The error is more affected by underestimation at high pressures and overestimation at low values. However, it remains between $13 - 16$ kPa as pressure increases from 50 kPa to 160 kPa. To obtain Figure 5(b), we sorted and divided pressure values into 50 bins, then reported the RMS error and average pressure for each bin.

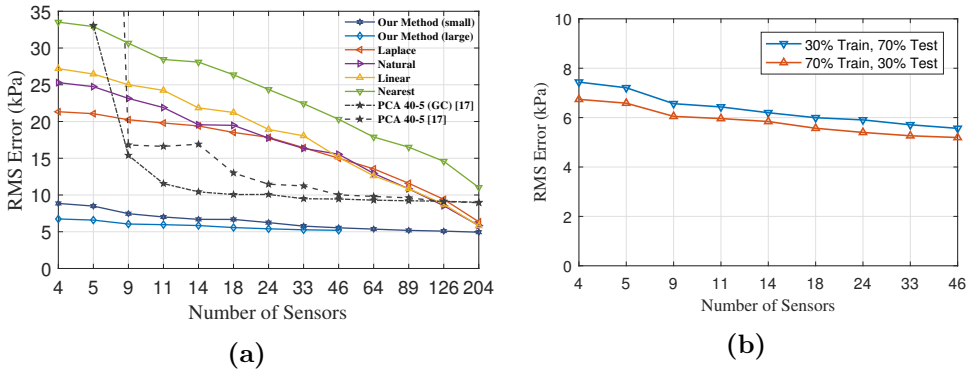

(a) **(b)**

Figure 6: (a) Error comparison between our method and interpolation techniques. We used 740×50 dictionaries, mK-SVD with $S = 2$ and both normal (small) and large sensors for our method.(b) Reconstruction error for 740×50 dictionaries learned with 30% of data. We used mK-SVD with $S = 2$ and OMP algorithm.

3.5.5 Comparison with interpolation techniques

We compared the performance of our data-driven approach with various interpolation methods commonly used in medical image processing: Laplace, Natural Neighbour, Linear, and Nearest Neighbour (Lehmann et al., 1999). We also applied the GMM-PCA based approach proposed in (Ostadabbas et al., 2014) to our dataset with its recommended settings using sensor locations at Gaussian centers (GC) as well as our sensor selection method. The results of the comparison in Figure 6(a) shows superiority of our approach over other techniques which clearly break down for small number of sensors.

3.5.6 Dictionary learning with limited training data

Finally, we examined the capability of our approach to work with limited training data. We used 30% of the data for training and the rest for test. The result is shown in Figure 6(b) using the mK-SVD with $S = 2$, OMP algorithm and large sensors. The error has increased at most by 0.7 kPa for $K = 4$ sensors, confirming that our approach still works well.

4. Conclusion

In this work, we proposed a spatially-continuous plantar pressure reconstruction technique specifically for $K < 10$ number of sensors based on CS principles. The key point in solving such highly under-determined system is to find a sparse representation for the underlying model. Our method takes advantage of high resolution training data to learn a dictionary in which pressure images are sparse, and then uses CS techniques to reconstruct images from sparsely placed, even much larger sensors. The proposed approach outperformed blind interpolation techniques such that the best method we tested, needed more than 170 sensors to give the same reconstruction accuracy we obtained with only 4 sensors. We also showed that our algorithm is robust in presences of measurement error and limited training data. In the reconstruction phase, we used classic OMP algorithm which can be efficiently implemented for realtime applications. Our method addresses both cost and energy constraints for practical in-shoe monitoring systems by providing high reconstruction accuracy using very small number of sensors with flexible size, and therefore ultimately can improve the quality of life of many individuals suffering from foot problems.

References

Moticon OpenGo Science, Scientific Foot Dynamics Analysis. http://www.moticon.de/products/science-research. Accessed: 2017.

PPS Foot Pressure Mapping System. http://www.pressureprofile.com/foot-pressure-mapping-system. Accessed: 2017.

SennoTech, Sensing Innovative. http://sennotech.com/EN/product/insole.php. Accessed: 2017.

Sensor Products Inc. (SPI) Tactile Pressure Experts. http://www.sensorprod.com/foot-plate-pressure-sensor.php. Accessed: 2017.

Tekscan Pressure and Force Measurement Technology. http://www.tekscan.com/sensor-technology. Accessed: 2017.

Abdul Hadi Abdul Razak, Aladin Zayegh, Rezaul K Begg, and Yufridin Wahab. Foot plantar pressure measurement system: a review. volume 12, pages 9884–9912. Molecular Diversity Preservation International, 2012.

Michal Aharon, Michael Elad, and Alfred Bruckstein. K-svd: An algorithm for designing overcomplete dictionaries for sparse representation. volume 54, pages 4311–4322. IEEE, 2006.

Emmanuel J Candès and Michael B Wakin. An introduction to compressive sampling. volume 25, pages 21–30. IEEE, 2008.

Darren Craven, Brian McGinley, Liam Kilmartin, Martin Glavin, and Edward Jones. Compressed sensing for bioelectric signals: a review. volume 19, pages 529–540. IEEE, 2015.

David L Donoho and Michael Elad. Optimally sparse representation in general (nonorthogonal) dictionaries via 1 minimization. volume 100, pages 2197–2202. National Acad Sciences, 2003.

David L Donoho, Yaakov Tsaig, Iddo Drori, and Jean-Luc Starck. Sparse solution of underdetermined systems of linear equations by stagewise orthogonal matching pursuit. volume 58, pages 1094–1121. IEEE, 2012.

Lawrence A Lavery, Edgar JG Peters, and David G Armstrong. What are the most effective interventions in preventing diabetic foot ulcers? volume 5, pages 425–433. Wiley Online Library, 2008.

Thomas Martin Lehmann, Claudia Gonner, and Klaus Spitzer. Survey: Interpolation methods in medical image processing. volume 18, pages 1049–1075. IEEE, 1999.

Benyuan Liu, Zhilin Zhang, Gary Xu, Hongqi Fan, and Qiang Fu. Energy efficient telemonitoring of physiological signals via compressed sensing: A fast algorithm and power consumption evaluation. volume 11, pages 80–88. Elsevier, 2014.

Sarah Ostadabbas, Mehrdad Nourani, and Matthew Pompeo. Continuous plantar pressure modeling using sparse sensors. pages 309–314. IEEE, 2012a.

Sarah Ostadabbas, Adnan Saeed, Mehrdad Nourani, and Matthew Pompeo. Sensor architectural tradeoff for diabetic foot ulcer monitoring. pages 6687–6690. IEEE, 2012b.

Sarah Ostadabbas, Mehrdad Nourani, Adnan Saeed, Rasoul Yousefi, and Matthew Pompeo. A knowledge-based modeling for plantar pressure image reconstruction. volume 61, pages 2538–2549. IEEE, 2014.

J Bradford Rice, Urvi Desai, Alice Kate G Cummings, Howard G Birnbaum, Michelle Skornicki, and Nathan B Parsons. Burden of diabetic foot ulcers for medicare and private insurers. volume 37, pages 651–658. Am Diabetes Assoc, 2014.

Robert Tibshirani. Regression shrinkage and selection via the lasso. pages 267–288. JSTOR, 1996.

Chikamune Wada, Yukinobu Sugimura, Futoshi Wada, Kenji Hachisuka, Takafumi Ienaga, Yoshihiko Kimuro, and Takunori Tsuji. Development of a rehabilitation support system with a shoe-type measurement device for walking. In *SICE Annual Conference 2010, Proceedings of*, pages 2534–2537. IEEE, 2010.

James Williamson, Qi Liu, Fenglong Lu, Wyatt Mohrman, Kun Li, Robert Dick, and Li Shang. Data sensing and analysis: Challenges for wearables. In *The 20th Asia and South Pacific Design Automation Conference*, pages 136–141. IEEE, 2015.

Wenyao Xu, Mi Zhang, Alexander A Sawchuk, and Majid Sarrafzadeh. Co-recognition of human activity and sensor location via compressed sensing in wearable body sensor networks. In *2012 Ninth International Conference on Wearable and Implantable Body Sensor Networks*, pages 124–129. IEEE, 2012.

Mi Zhang and Alexander A Sawchuk. Human daily activity recognition with sparse representation using wearable sensors. volume 17, pages 553–560. IEEE, 2013.